Journal of Alloys and Compounds 521 (2012) 95–100

Contents lists available at SciVerse ScienceDirect

Journal of Alloys and Compounds

journal homepage: www.elsevier.com/locate/jallcom

Co_3O_4 nanowires as high capacity anode materials for lithium ion batteries

Xiayin Yao, Xing Xin, Yiming Zhang, Jun Wang, Zhaoping Liu*, Xiaoxiong Xu**

Ningbo Institute of Material Technology & Engineering, Chinese Academy of Sciences, Ningbo 315201, PR China

ARTICLE INFO

Article history:
Received 4 October 2011
Received in revised form 7 January 2012
Accepted 9 January 2012
Available online 16 January 2012

Keywords:
Co_3O_4 nanowires
High capacity
Good capacity retention
Anode materials
Lithium-ion batteries

ABSTRACT

Co_3O_4 nanowires were synthesized from the decomposition of $CoC_2O_4{\cdot}2H_2O$ nanowires which were obtained through a polyvinyl alcohol (PVA)-assisted solution-based precipitation process. And the formation mechanism of $CoC_2O_4{\cdot}2H_2O$ nanowires was discussed. The Co_3O_4 nanowires had diameters in the range of 30–60 nm and lengths of several micrometers, inheriting the morphology of the $CoC_2O_4{\cdot}2H_2O$ nanowires. The Co_3O_4 nanowires as an anode material in lithium-ion batteries exhibited a stable specific discharge/charge capacity of 611 mAh/g and 598 mAh/g after fifty cycles at a current density of 0.11 A/g, which were much higher than that of commercial Co_3O_4 nanoparticles. In addition, the charge capacity of the as-synthesized Co_3O_4 nanowires was more than two times higher than that of the commercial Co_3O_4 nanoparticles at a current density of 1.1 A/g. These results indicate that the as-prepared Co_3O_4 nanowires have potential to be a promising candidate as high capacity anode material in the next generation lithium-ion batteries.

1. Introduction

Rechargeable lithium-ion batteries have been widely used as the state-of-the-art and dominant power source for portable electronic devices [1]. The electrode materials play a vital role both in the currently used lithium-ion batteries and the next generation lithium-ion batteries developing for the practical applications in hybrid electric vehicles (HEVs) and electric vehicles (EVs). Great efforts have been made to develop alternative anode materials for lithium-ion batteries with improved electrochemical properties [2–4]. The employment of nanosized and nanostructured materials provides new opportunities for rechargeable lithium-ion batteries with higher energy density and better cycling stability [5–9]. Specially, one-dimensional (1D) nanostructured transition metal oxides have received much attention since they can provide short pathways and high kinetics for lithium ion insertion/extraction [10,11]. Hence, it is anticipated that the 1D nanostructured electrode materials would exhibit higher reactivity, which would no doubt enhance the electrochemical performances of the electrode materials.

Co_3O_4, which can deliver as high as three times the capacity of graphite (theoretical capacity of 372 mAh/g), has been reported to be a promising anode material for the next generation lithium-ion batteries [12–16]. Until now, several methods have been developed to prepare 1D nanostructured Co_3O_4, including hydrothermal approach [17–19], template method [20–22], microemulsion-based route [23,24], and electrospinning strategy [25]. However, these available methods have great difficulties to produce 1D nanostructured Co_3O_4 in large-scale.

In this study, we present a facile method to synthesize Co_3O_4 nanowires from decomposition of $CoC_2O_4{\cdot}2H_2O$ nanowires. The electrochemical properties of the as-obtained Co_3O_4 nanowires were evaluated. This strategy showed us a facile procedure for realizing large-scale production of Co_3O_4 nanowires with improved electrochemical performance. For the purpose of comparison, a commercial Co_3O_4 was investigated in this study as well.

2. Experimental

2.1. Synthesis of $CoC_2O_4{\cdot}2H_2O$ and Co_3O_4 nanowires

All of the chemicals were analytical grade and used without further purification. The Co_3O_4 nanowires were synthesized from the decomposition of $CoC_2O_4{\cdot}2H_2O$ nanowires. The $CoC_2O_4{\cdot}2H_2O$ precursors were firstly prepared through a solution-based direct precipitation process using polyvinyl alcohol (PVA, with the degree of polymerization DP = 1750 ± 50) as surfactant. In a typical procedure, 15 g of 33.3 wt% $CoSO_4{\cdot}7H_2O$ aqueous solution was firstly mixed with 30 g of PVA aqueous solution under stirring at room temperature. The concentrations of PVA aqueous solution were set at 0 wt%, 0.2 wt% and 1.0 wt%, respectively. And then, 11.2 g of 20 wt% $H_2C_2O_4{\cdot}2H_2O$ aqueous solution was introduced into the above solution. Pink precipitates appeared immediately. After stirring for 5 min, the as-prepared $CoC_2O_4{\cdot}2H_2O$ precipitate was centrifugalized and washed for several times with deionized water, and dried in vacuum. Finally, the $CoC_2O_4{\cdot}2H_2O$ precursors were calcined at 600 °C for 2 h in air to obtain Co_3O_4 nanowires.

2.2. Characterizations

Scanning electron microscopy (SEM) images were acquired with a Hitachi S-4800 field emission scanning electron microscope. The samples were coated with a

* Corresponding author. Tel.: +86 574 86685096; fax: +86 574 86685096.
** Corresponding author. Tel.: +86 574 86685701; fax: +86 574 86685701.
E-mail addresses: liuzp@nimte.ac.cn (Z. Liu), xuxx@nimte.ac.cn (X. Xu).

0925-8388/$ – see front matter © 2012 Elsevier B.V. All rights reserved.
doi:10.1016/j.jallcom.2012.01.047

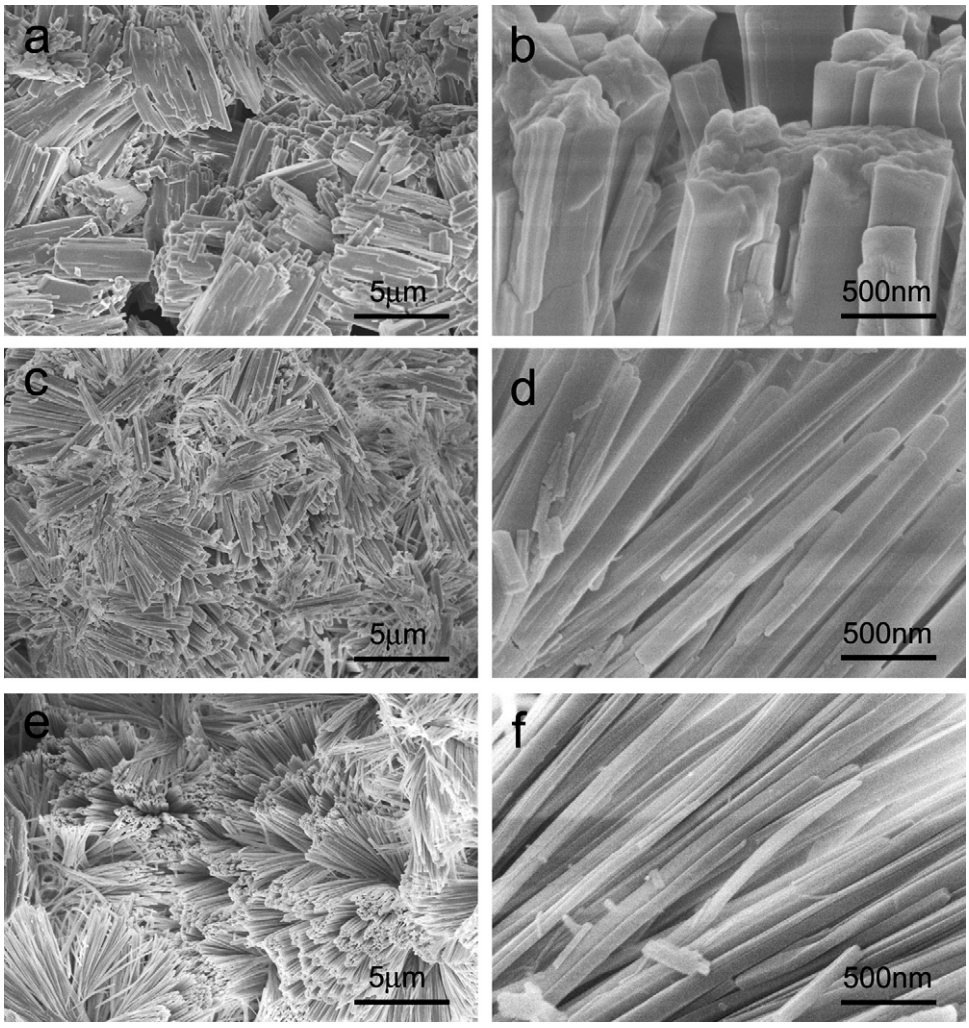

Fig. 1. SEM images of $CoC_2O_4{\cdot}2H_2O$ precursors synthesized with various PVA aqueous solution concentrations: (a and b) 0 wt%, (c and d) 0.2 wt%, and (e and f) 1 wt%.

thin layer of platinum before the SEM examination. X-ray diffraction (XRD) patterns were obtained on a D8-Advance (Bruker AXS, Germany) powder diffractometer with Cu Kα radiation (λ = 1.54178 Å), operating at a voltage of 40 kV and scanning from 10° to 70°. X-ray photoelectron spectra (XPS) were collected on a Kratos AXIS ULTRA^{DLD} X-ray photoelectron spectrometer. Transmission electron microscopy (TEM) experiments were performed on an FEI Tecnai G^2 F20 transmission electron microscopy at an accelerating voltage of 200 kV. The Brunauer–Emmett–Teller (BET) tests were determined via a Micromeritics ASAP-2020M nitrogen adsorption apparatus. Pore size distribution plots were obtained by the Barrett-Joyner-Halenda (BJH) method.

The electrochemical performances were evaluated with a standard CR2032 coin cell using lithium metal as counter and reference electrodes, Celgard 2600 as the separator, and 1 M $LiPF_6$ (dissolved in ethylene carbonate and dimethyl carbonate with a 1:1 volume ratio) as the electrolyte. The working electrodes were fabricated by mixing Co_3O_4 nanowires (80 wt%), Super P (15 wt%) and poly(vinylidene fluoride) (5 wt%) in N-methyl-2-pyrrolidone to form uniform slurry. The obtained slurry was spread on Cu foil, dried in vacuum and pressed to obtain the working electrode. The loading density of the electrode is about 3 mg cm^{-2}. And the morphology of Co_3O_4 nanowires can be maintained after electrode preparation. Cells were galvanostatically cycled at room temperature using a LAND-CT2001A battery test system (Jinnuo Wuhan Corp., China) within the voltage range of 0.01 and 3.0 V (vs. Li^+/Li). Cyclic voltammetry measurements were performed on an Autolab PGSTAT302N electrochemical workstation (Metrohm, Switzerland) at 0.1 mV/s in the voltage range of 0.01–3.0 V.

3. Results and discussion

The SEM images of $CoC_2O_4{\cdot}2H_2O$ precursors, synthesized with various PVA aqueous solution concentrations, were shown in Fig. 1. With the increasing of PVA concentration, the morphology of $CoC_2O_4{\cdot}2H_2O$ was gradually converted to the nanowires. In the case of 1.0 wt% PVA concentration, the as-obtained $CoC_2O_4{\cdot}2H_2O$ precursor exhibited the morphology of nanowires with smooth surface and having the diameter range of 50–100 nm and the length of several micrometers (Fig. 1e and f). It is worth stating that the morphology of $CoC_2O_4{\cdot}2H_2O$ slightly changed with further increasing PVA concentration.

Based on the SEM results, we can speculate that the PVA plays an important role in the nucleation and growing process to control the size and orientation of the $CoC_2O_4{\cdot}2H_2O$, and that the PVA

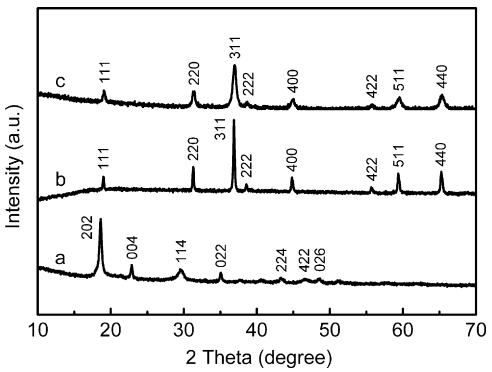

Fig. 2. XRD patterns of the as-synthesized (a) $CoC_2O_4{\cdot}2H_2O$ nanowires, (b) Co_3O_4 nanowires and (c) the commercial Co_3O_4 nanoparticles.

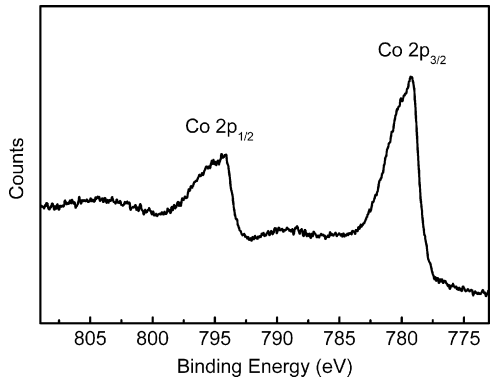

Fig. 3. XPS pattern of the as-prepared Co_3O_4 nanowires.

concentration in the system has a strong influence on the morphology of $CoC_2O_4{\cdot}2H_2O$. It has been previously reported that PVA is an effective surfactant for preparing 1D nanomaterials because the OH ligands on the PVA chains can chelate with metal cations leading to the anisotropic growth of a solid material [26–29]. Herein, similar principles can be applied to explain the formation of $CoC_2O_4{\cdot}2H_2O$ nanowires using PVA-assisted solution-based precipitation process. In the precursor solution, cobalt ions were firstly adsorbed into PVA chains and formed Co^{2+}–PVA complex with OH ligands. After corresponding amount of $H_2C_2O_4{\cdot}2H_2O$ aqueous solution was introduced into the precursor solution, the Co^{2+}–PVA was immediately transformed into $CoC_2O_4{\cdot}2H_2O$–PVA complex, which was confirmed by the rapid formation of pink color precipitation. Finally, $CoC_2O_4{\cdot}2H_2O$ seeds grew up to form 1D nanostructures with the confinement of the PVA carbon backbone grids. In addition, the $CoC_2O_4{\cdot}2H_2O$ crystal nucleus could be adjusted by the size of grids formed with PVA chains controlled by the PVA concentration in the aqueous solution, so the $CoC_2O_4{\cdot}2H_2O$ could be obtained with different diameters and lengths, as shown in Fig. 1c and e. There is no denying the fact that PVA has virtual roles on both the confinement of the growth units' diameter and length and the 1D orientation growth of $CoC_2O_4{\cdot}2H_2O$ nanowires during the nucleation and growing process.

Fig. 2 showed the XRD patterns of the as-synthesized $CoC_2O_4{\cdot}2H_2O$ nanowires, the Co_3O_4 nanowires and the commercial Co_3O_4. All diffraction peaks in Fig. 2a can be indexed to the orthorhombic phase of $CoC_2O_4{\cdot}2H_2O$ (JCPDS No. 25-0250). After the heat-treatment at 600 °C for 2 h in air, the $CoC_2O_4{\cdot}2H_2O$ nanowires were turned into cubic structure corresponding to Co_3O_4 phase (JCPDS No. 42-1467) (Fig. 2b). No diffraction peaks due to impure phases were observed, indicating that the highly pure samples were obtained. The commercial Co_3O_4 (Fig. 2c) has the same crystal structure as that of the Co_3O_4 nanowires. Moreover, XPS measurement further confirmed the formation of Co_3O_4 nanowires. It can be seen in Fig. 3that the main Co 2p photoelectron peaks are located at 779.3 and 794.5 eV with shake-up satellite peaks at 789.5 and 804.5 eV, corresponding to the characteristic peaks of Co_3O_4 [30].

The SEM images of the Co_3O_4 nanowires, prepared by the heat-treatment of $CoC_2O_4{\cdot}2H_2O$ nanowires, was shown in Fig. 4a and b. It can be seen that the as-obtained Co_3O_4 maintained the morphology of the $CoC_2O_4{\cdot}2H_2O$ precursor and showed a 1D nanowire characteristic (Fig. 4a). However, the surface of the Co_3O_4 nanowires became rough and displayed a loose structure consisting of interconnected nanoparticles, as shown in Fig. 4b. Different from the Co_3O_4 nanowires, the commercial Co_3O_4 showed a micro–nano structure (Fig. 4c) and had a spherical morphology with particle sizes in the range of 1–2 μm. These micro-spherical particles were composed of primary nanoparticles with average grain-size of about 30 nm (Fig. 4d).

In order to further study the structure of Co_3O_4 nanowires, TEM, HRTEM and selected area electron diffraction (SAED) experiments were carried out as well. It is clear to see from the TEM images (Fig. 5a and b) that the diameter of the Co_3O_4 nanowires had decreased to 30–60 nm, which was ascribe to the decomposition of the oxalate group in $CoC_2O_4{\cdot}2H_2O$ precursor. The SAED pattern of a nanograin in the Co_3O_4 nanowires (the insert in Fig. 5b) presented intense reflection spots of cubic structure Co_3O_4, which agreed well with the XRD pattern. The HRTEM image in Fig. 5c showed the microstructure of the individual grains. The spacing

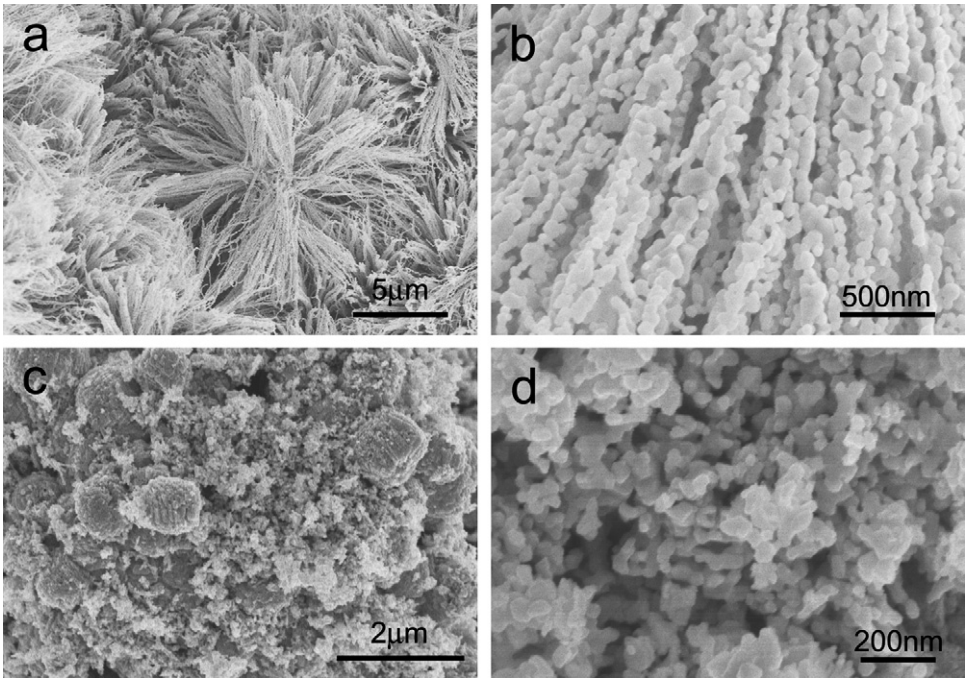

Fig. 4. SEM images of (a and b) the Co_3O_4 nanowires and (c and d) the commercial Co_3O_4 nanoparticles.

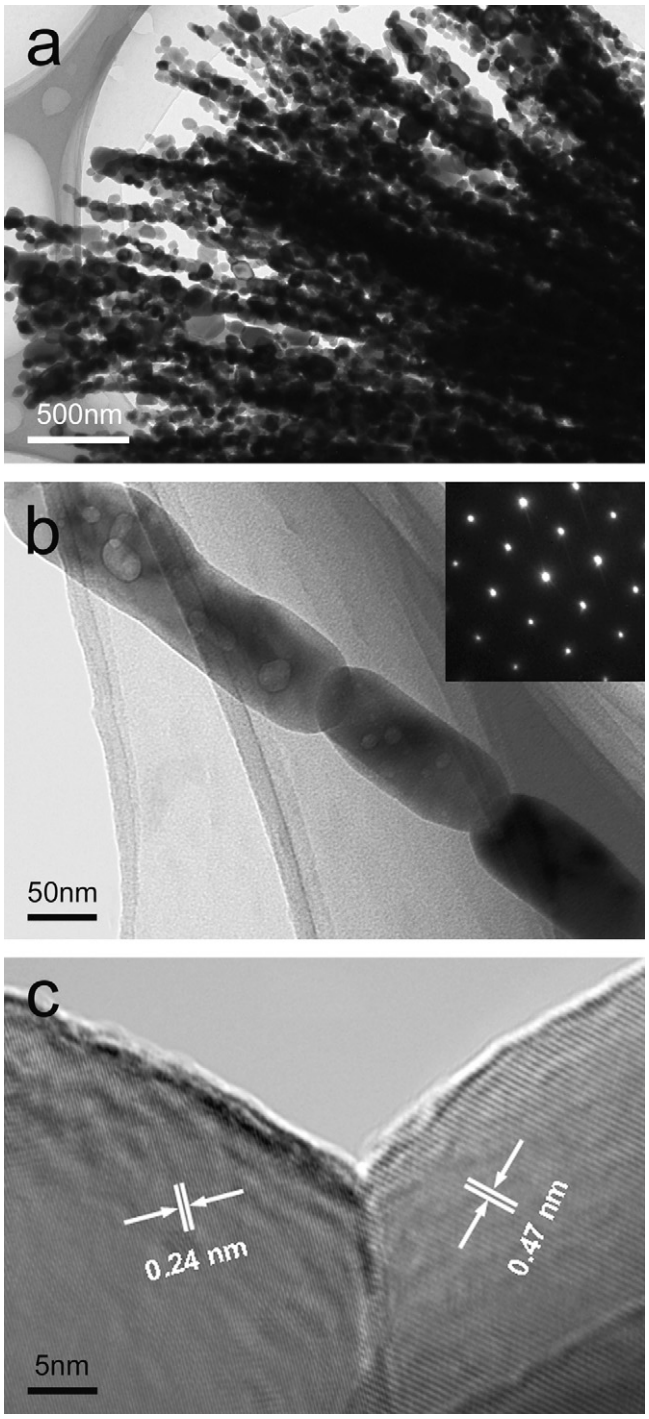

Fig. 5. TEM (a and b) and HRTEM (c) images of the Co_3O_4 nanowires, the insert was the corresponding SAED pattern.

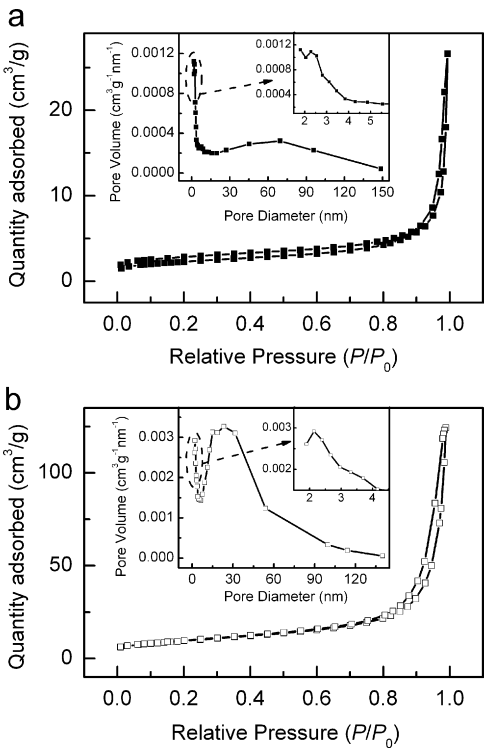

Fig. 6. The nitrogen adsorption–desorption isotherms of (a) the as-obtained Co_3O_4 nanowires and (b) the commercial Co_3O_4 nanoparticles. The inserts were the corresponding BJH pore size distribution curves.

of the lattice planes in the image were determined as 0.47 nm and 0.24 nm, which were consistent with the standard values for the (1 1 1) and (3 1 1) planes, respectively.

To examine the specific surface area and the pore size distribution, N_2 adsorption–desorption isothermal measurements were performed. The results were shown in Fig. 6 and the inserts were the corresponding BJH pore size distribution curves. It can be seen that the Co_3O_4 nanowires possessed bimodal pore size distribution of ca. 2.5 nm and 68 nm (the insert in Fig. 6a). The appearance of small pores were apparently caused by the release of CO_2 during the decomposition of $CoC_2O_4{\cdot}2H_2O$ [24], and the large ones may be formed by the aggregation of the nanowires, i.e. the interspaces in Co_3O_4 nanowire nanostructures. The similar pore size distribution style (the insert in Fig. 6b) was observed for the commercial Co_3O_4 nanoparticles. The porous structure would be of beneficial to the electrochemical lithium storage. The surface areas estimated from the BET method are 8.0 m^2/g for the Co_3O_4 nanowires and 34.2 m^2/g for the commercial Co_3O_4 nanoparticles.

Cyclic voltammetry measurements were performed to elucidate the electrochemical process of the Co_3O_4 electrodes at a scan rate of 0.1 mV/s between 0.01 and 3.0 V, as shown in Fig. 7. For the as-synthesized Co_3O_4 nanowires electrode, there is a high-intensity reduction peak at around 0.95 V during the cathodic process in the first cycle (Fig. 7a), which can be ascribed to the initial reduction of Co_3O_4 to metallic cobalt, accompanying with the electrochemical formation of amorphous Li_2O, as well as a partially irreversible solid electrolyte interphase (SEI) layer [31,32]. Meanwhile, an oxidation peak at about 2.1 V was recorded during the anodic process, corresponding to the oxidation of metallic Co to Co_3O_4 and the decomposition of Li_2O [33,34]. The commercial Co_3O_4 nanoparticles electrode showed similar cyclic voltammograms in the first cycle except for one weak shoulder peak at 1.2 V during the cathodic process (Fig. 7b), which was generally attributed to the reduction of the Co_3O_4 to CoO (or $Li_xCo_3O_4$) [33]. From the second cycle, the reduction peak shifted to a higher potential at about 1.13 V, which might be related to the pulverization of the Co_3O_4 [35,36]. It is generally accepted that the mechanisms for these reactions are the reversible reactions between Co_3O_4 and Co/Li_2O, and the partial composition/decomposition of the electrolytical coating on the surface of Co_3O_4 [37,38]. The overall electrochemical processes can be expressed as follows:

$$Co_3O_4 + 8Li^+ + 8e^- \underset{\text{Charge}}{\overset{\text{Discharge}}{\rightleftharpoons}} 3Co + 4Li_2O$$

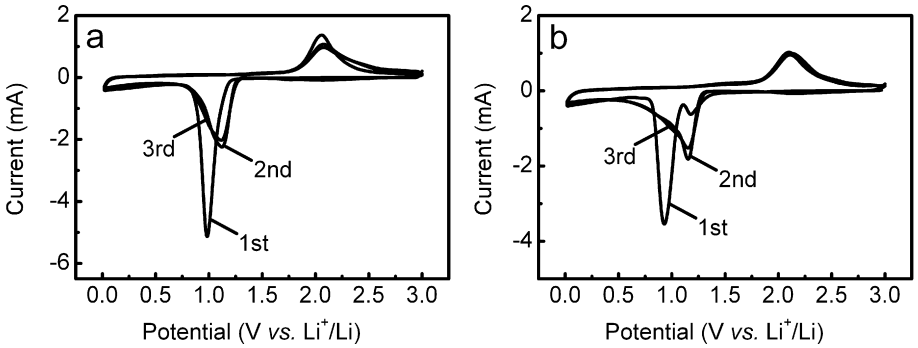

Fig. 7. Cyclic voltammograms of (a) the Co_3O_4 nanowires and (b) the commercial Co_3O_4 nanoparticles electrodes at a scan rate of 0.1 mV/s between 0.01 and 3.0 V.

The electrochemical performance of the as-synthesized Co_3O_4 nanowires with respect to Li^+-ion insertion/extraction was investigated in half cells by galvanostatic charge/discharge testing in the voltage window of 0.01–3.0 V. Fig. 8 showed the voltage profile, the cycling behavior and the Coulombic efficiency of the samples at a constant current density of 0.11 A/g. It can be seen that the Co_3O_4 nanowire electrode materials exhibited the discharge potential plateau at around 1.12 V, and delivered an initial discharge capacity of 1027 mAh/g and charge capacity of 755 mAh/g, with a Coulombic efficiency of 73.5%. A large capacity loss between the 1st and 2nd cycles was observed, which was due to the formation of a solid electrolyte interphase layer on the electrode surface during the 1st discharge process [17,39]. Up to the 50th cycle, the discharge/charge capacity remained about 611 mAh/g and 598 mAh/g, respectively, which is much higher than that of the commercial anode materials (graphite, 372 mAh/g) and those recently reported in Refs. [32,37,39,40]. Compared with those of Co_3O_4 nanowires, the commercial Co_3O_4 showed a slightly higher discharge/charge capacity of about 1137 mAh/g and 881 mAh/g with a Coulombic efficiency of 77.5% for the first cycle. This could originate from larger surface area of the commercial Co_3O_4 nanoparticles, providing more sites for lithium ion intercalation/deintercalation. However, after fifty cycles, the discharge/charge capacity rapidly degraded to about 145 mAh/g and 140 mAh/g, respectively. Clearly, the as-synthesized Co_3O_4 nanowires exhibited much better capacity retention than that of the commercial Co_3O_4 nanoparticles. The reason could be that the 1D nanostructure of Co_3O_4 nanowires facilitates the alleviation of the mechanical stress induced by volume change during repeated charge–discharge cycles [11]. The superior lithium storage capability of the as-obtained Co_3O_4 nanowires shed light on a potential application as an anode material in next generation lithium-ion batteries with high energy density and long cycling life.

Fig. 9 showed the rate capabilities of the two anode materials, i.e. the as-synthesized Co_3O_4 nanowires and the commercial Co_3O_4 nanoparticles, under various current densities ranging from 0.22 to 1.1 A/g. As the current density was increased, the discharge/charge capacities of the two anode materials decreased evidently and the charge capacities maintained at 64.8% for the as-synthesized Co_3O_4 nanowires and 26.6% for the commercial Co_3O_4 nanoparticles on the basis of the value at 0.22 A/g. In addition, for the reversible capacity, the charge capacity of the as-synthesized Co_3O_4 nanowires was more than two times higher than that of the commercial Co_3O_4 nanoparticles at a current density of 1.1 A/g. Apparently, the as-synthesized Co_3O_4 nanowires possessed excellent high-rate capability compared with that of the commercial

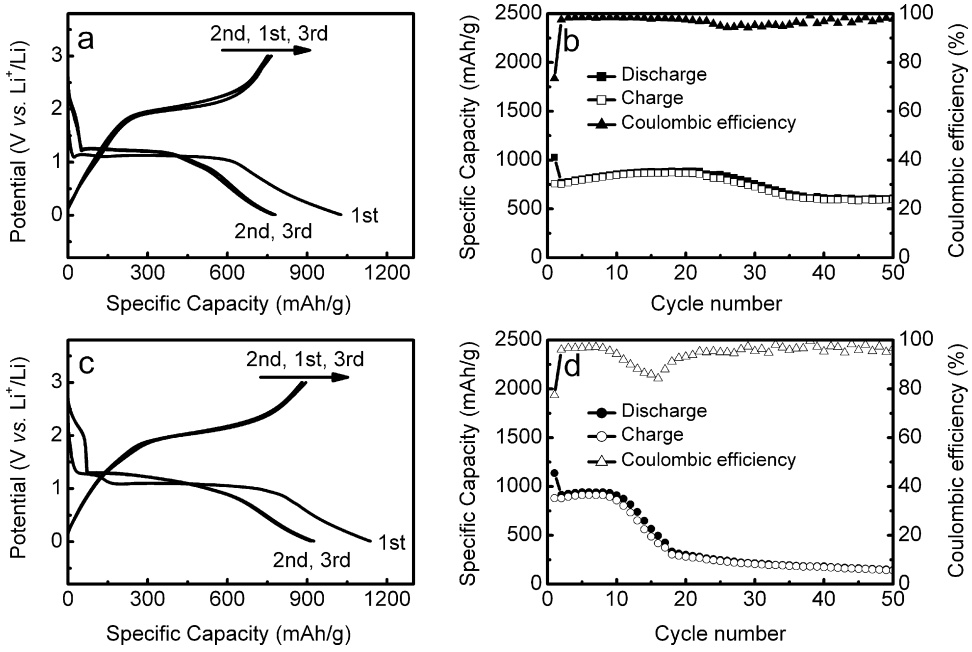

Fig. 8. Galvanostatic charge/discharge profiles, cycling performance and the Coulombic efficiency of (a and b) the Co_3O_4 nanowires and (c and d) the commercial Co_3O_4 nanoparticles electrodes discharged/charged at a constant current density of 0.11 A/g.

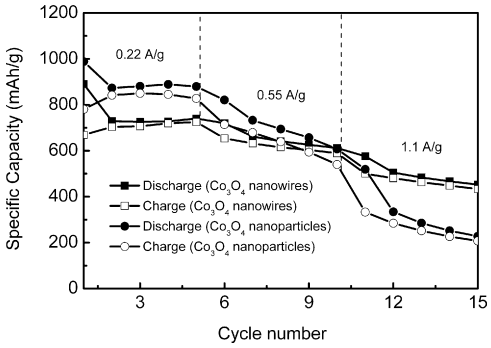

Fig. 9. Rate capabilities of the as-synthesized Co_3O_4 nanowires and the commercial Co_3O_4 nanoparticles electrodes under various current densities.

Co_3O_4 nanoparticles. However, it is worth noting that the rate performances of the two anode materials need to be further improved in order to meet the challenge in the new generation lithium-ion batteries with higher power density. Further works on this issue are desirable and it is hoped that we would achieve this in the coming time.

4. Conclusions

We have presented a facile and effective route for synthesizing nanostructured Co_3O_4 nanowires from decomposition of $CoC_2O_4{\cdot}2H_2O$, and it can be employed for large-scale production. The formation mechanism of $CoC_2O_4{\cdot}2H_2O$ nanowires was proposed. The as-obtained Co_3O_4 nanowires with diameters in the range of 30–60 nm came into the morphology of $CoC_2O_4{\cdot}2H_2O$ nanowires. The as-synthesized Co_3O_4 nanowires, employed as the anode material of lithium-ion battery, delivered a discharge/charge capacity of 611 mAh/g and 598 mAh/g after fifty cycles at a current density of 0.11 A/g, which was much higher than those of commercial Co_3O_4 nanoparticles. In addition, the as-synthesized Co_3O_4 nanowires possessed excellent high-rate capability compared to the commercial Co_3O_4 nanoparticles. The excellent electrochemical performances could be attributed to the alleviation of the mechanical stress induced by the volume change during the repeated lithiation/delithiation processes for the 1D nanostructured feature of Co_3O_4 nanowires, which make them promising for applications requiring batteries with high energy density and long cycling life.

Acknowledgements

We are grateful for financial support from the National Natural Science Foundation of China (Grant No. 51172250), Zhejiang Provincial Natural Science Foundation of China (Grant Nos. R4100194 and Y4100499), and the Natural Science Foundation of Ningbo (Grant No. 2011A610201).

References

[1] M. Armand, J.M. Tarascon, Nature 451 (2008) 652–657.
[2] C. Liu, F. Li, L.P. Ma, H.M. Cheng, Adv. Mater. 22 (2010) E28–E62.
[3] F.Y. Cheng, J. Liang, Z.L. Tao, J. Chen, Adv. Mater. 23 (2011) 1695–1715.
[4] H. Li, Z.X. Wang, L.Q. Chen, X.J. Huang, Adv. Mater. 21 (2009) 4593–4607.
[5] Y.G. Wang, H.Q. Li, P. He, E. Hosono, H.S. Zhou, Nanoscale 2 (2010) 1294–1305.
[6] N. Sivakumar, S.R.P. Gnanakan, K. Karthikeyan, S. Amaresh, W.S. Yoon, G.J. Park, Y.S. Lee, J. Alloys Compd. 509 (2011) 7038–7041.
[7] L.W. Ji, Z. Lin, M. Alcoutlabi, X.W. Zhang, Energy Environ. Sci. 4 (2011) 2682–2699.
[8] F. Wang, W.Z. Tao, M.S. Zhao, M.W. Xu, S.C. Yang, Z.B. Sun, L.Q. Wang, X.P. Song, J. Alloys Compd. 509 (2011) 9798–9803.
[9] J.R. Szczech, S. Jin, Energy Environ. Sci. 4 (2011) 56–72.
[10] C.M. Park, J.H. Kim, H. Kim, H.J. Sohn, Chem. Soc. Rev. 39 (2010) 3115–3141.
[11] J.A. Jiang, Y.Y. Li, J.P. Liu, X.T. Huang, Nanoscale 3 (2011) 45–58.
[12] P. Poizot, S. Laruelle, S. Grugeon, L. Dupont, J.M. Tarascon, Nature 407 (2000) 496–499.
[13] W. Wen, J.M. Wu, J.P. Tu, J. Alloys Compd. 513 (2012) 592–596.
[14] Z.W. Fu, Y. Wang, Y. Zhang, Q.Z. Qin, Solid State Ionics 170 (2004) 105–109.
[15] B. Wang, Y. Wang, J. Park, H. Ahn, G.X. Wang, J. Alloys Compd. 509 (2011) 7778–7783.
[16] M.M. Thackeray, S.D. Baker, K.T. Adendorff, J.B. Goodenough, Solid State Ionics 17 (1985) 175–181.
[17] G.X. Wang, X.P. Shen, J. Yao, J. Power Sources 189 (2009) 543–546.
[18] W.H. Li, Mater. Lett. 62 (2008) 4149–4151.
[19] J.H. Yang, H. Hyodo, K. Kimura, T. Sasaki, Nanotechnology 21 (2010) 045605.
[20] G.B. Ji, Z.H. Gong, W.X. Zhu, M.B. Zheng, S.T. Liao, K. Shen, J.S. Liu, J.M. Cao, J. Alloys Compd. 476 (2009) 579–583.
[21] K.M. Shaju, F. Jiao, A. Debart, P.G. Bruce, Phys. Chem. Chem. Phys. 9 (2007) 1837–1842.
[22] T. Li, S.G. Yang, L.S. Huang, B.X. Gu, Y.W. Du, Nanotechnology 15 (2004) 1479–1482.
[23] R. Xu, J.W. Wang, Q.Y. Li, G.Y. Sun, E.B. Wang, S.H. Li, J.M. Gu, M.L. Ju, J. Solid State Chem. 182 (2009) 3177–3182.
[24] N. Du, Y.F. Xu, H. Zhang, C.X. Zhai, D.R. Yang, Nanoscale Res. Lett. 5 (2010) 1295–1300.
[25] Y.H. Ding, P. Zhang, Z.L. Long, Y. Jiang, J.N. Huang, W.J. Yan, G. Liu, Mater. Lett. 62 (2008) 3410–3412.
[26] W.B. Sang, Y.Y. Fang, J.R. Fan, Y. He, J.H. Min, Y.B. Qian, J. Cryst. Growth 299 (2007) 272–276.
[27] Z.Y. Wang, B.B. Huang, X.Y. Qin, X.Y. Zhang, P. Wang, J.Y. Wei, J.Y. Zhan, X.Y. Jing, H.X. Liu, Z.H. Xu, H.F. Cheng, X.N. Wang, Z.K. Zheng, Mater. Lett. 63 (2009) 130–132.
[28] Y. He, W.B. Sang, J.A. Wang, R.F. Wu, J.H. Min, Mater. Chem. Phys. 94 (2005) 29–33.
[29] Y.M. Hu, H.S. Gu, D. Zhou, Z. Wang, H.L.W. Chan, Y. Wang, J. Am. Ceram. Soc. 93 (2010) 609–613.
[30] T.J. Chuang, C.R. Brundle, D.W. Rice, Surf. Sci. 59 (1976) 413–429.
[31] P. Poizot, S. Laruelle, S. Grugeon, L. Dupont, J.M. Tarascon, J. Power Sources 97–98 (2001) 235–239.
[32] M.M. Rahman, J.Z. Wang, X.L. Deng, Y. Li, H.K. Liu, Electrochim. Acta 55 (2009) 504–510.
[33] D. Larcher, G. Sudant, J.B. Leriche, Y. Chabre, J.M. Tarascon, J. Electrochem. Soc. 149 (2002) A234–A241.
[34] J.Q. Wang, B. Niu, G.D. Du, R. Zeng, Z.X. Chen, Z.P. Guo, S.X. Dou, Mater. Chem. Phys. 126 (2011) 747–754.
[35] W.L. Yao, J. Yang, J.L. Wang, L.A. Tao, Electrochim. Acta 53 (2008) 7326–7330.
[36] H.J. Liu, S.H. Bo, W.J. Cui, F. Li, C.X. Wang, Y.Y. Xia, Electrochim. Acta 53 (2008) 6497–6503.
[37] Y. Liu, C.H. Mi, L.H. Su, X.G. Zhang, Electrochim. Acta 53 (2008) 2507–2513.
[38] V. Pralong, J.B. Leriche, B. Beaudoin, E. Naudin, M. Morcrette, J.M. Tarascon, Solid State Ionics 166 (2004) 295–305.
[39] J.G. Kang, Y.D. Ko, J.G. Park, D.W. Kim, Nanoscale Res. Lett. 3 (2008) 390–394.
[40] G.X. Wang, Y. Chen, K. Konstantinov, J. Yao, J.H. Ahn, H.K. Liu, S.X. Dou, J. Alloys Compd. 340 (2002) L5–L10.